

# Linköping University Post Print

## Thermoelectric transport properties of highly oriented FeSb<sub>2</sub> thin films

Y Sun, S Johnsen, Per Eklund, M Sillassen, J Bottiger, N Oeschler,  
P Sun, F Steglich and B B Iversen

N.B.: When citing this work, cite the original article.

Original Publication:

Y Sun, S Johnsen, Per Eklund, M Sillassen, J Bottiger, N Oeschler, P Sun, F Steglich and B B Iversen, Thermoelectric transport properties of highly oriented FeSb<sub>2</sub> thin films, 2009, JOURNAL OF APPLIED PHYSICS, (106), 3, 033710.

<http://dx.doi.org/10.1063/1.3155800>

Copyright: American Institute of Physics

<http://www.aip.org/>

Postprint available at: Linköping University Electronic Press

<http://urn.kb.se/resolve?urn=urn:nbn:se:liu:diva-20403>

# Thermoelectric transport properties of highly oriented FeSb<sub>2</sub> thin films

Y. Sun,<sup>1</sup> S. Johnsen,<sup>1</sup> P. Eklund,<sup>2,3</sup> M. Sillassen,<sup>2</sup> J. Böttiger,<sup>2</sup> N. Oeschler,<sup>4</sup> P. Sun,<sup>4</sup> F. Steglich,<sup>4</sup> and B. B. Iversen<sup>1,a)</sup><sup>1</sup>Centre for Energy Materials, Department of Chemistry and iNANO, University of Aarhus, DK-8000 Aarhus C, Denmark<sup>2</sup>Department of Physics and Astronomy and iNANO, University of Aarhus, DK-8000 Aarhus C, Denmark<sup>3</sup>Department of Physics, Chemistry, and Biology (IFM), Thin Film Physics Division, Linköping University, SE-581 83 Linköping, Sweden<sup>4</sup>Max Planck Institute for Chemical Physics of Solids, 01187 Dresden, Germany

(Received 26 April 2009; accepted 25 May 2009; published online 12 August 2009)

Highly textured FeSb<sub>2</sub> films were produced on quartz wafers by a sputtering method. Their resistivity and Seebeck coefficient ( $S$ ) were measured and a maximum absolute value of  $S \sim 160 \mu\text{V K}^{-1}$  at 50 K was obtained. Hall measurements were employed to study the charge carrier concentrations and Hall mobilities of the FeSb<sub>2</sub> films. By comparing with the transport properties of FeSb<sub>2</sub> single crystals and an extrinsically doped FeSb<sub>1.98</sub>Te<sub>0.02</sub> single crystal, the thermoelectric properties of the FeSb<sub>2</sub> films are demonstrated to be dominated by the intrinsic properties of FeSb<sub>2</sub> at a high charge carrier concentration. © 2009 American Institute of Physics.

[DOI: 10.1063/1.3155800]

## I. INTRODUCTION

Due to their promising applications for both solid state power generators and cooling devices, thermoelectric materials (TMs) have stimulated worldwide interest for many years.<sup>1-3</sup> The efficiency of TMs is evaluated using the dimensionless figure of merit, i.e.,  $ZT = S^2T/\rho\kappa$ , where  $S$ ,  $T$ ,  $\rho$ , and  $\kappa$  are the Seebeck coefficient, absolute temperature, resistivity, and thermal conductivity, respectively. To make a thermoelectric device commercially competitive, TMs with  $ZT$  values significantly higher than one are required. However, TMs with  $ZT \sim 1$  are still relatively few, especially for the TMs working below 200 K. Although there is a need for thermoelectric refrigeration, e.g., for refrigeration of superconductors in power cables, only few useful TMs working at low temperature have been found in the past 40 years.<sup>4-6</sup>

The strongly correlated semiconductor FeSb<sub>2</sub> is a promising TM.<sup>7,8</sup> Polycrystalline FeSb<sub>2</sub>, FeSb<sub>2-x</sub>Sn<sub>x</sub>, and FeSb<sub>2-x</sub>Te<sub>x</sub> have been explored and shown to have moderate thermoelectric performance.<sup>9-11</sup> In our previous work, we reported that single crystals of FeSb<sub>2</sub> exhibit colossal Seebeck coefficients ( $\sim 45\,000 \mu\text{V/K}$ ) and record high power factors ( $P = S^2/\rho$ ) of  $\sim 2300 \mu\text{W K}^{-2} \text{cm}^{-1}$  at 12 K,<sup>12</sup> which is 65 times larger than that of the state-of-the-art Bi<sub>2</sub>Te<sub>3</sub>-based TMs.<sup>13</sup> This emphasizes the potential of FeSb<sub>2</sub> for thermoelectric cooling at cryogenic temperature. It is the large lattice thermal conductivity ( $\kappa_L$ ) of bulk FeSb<sub>2</sub> that restricts its thermoelectric performance. In the past decade, reduction in  $\kappa_L$  has been demonstrated as the most important and effective strategy to improve  $ZT$  of TMs in both complex bulk materials<sup>14-16</sup> and low-dimensional materials systems.<sup>17-21</sup> The calculated mean free path of the dominant phonons of FeSb<sub>2</sub> at 12 K is  $\sim 100 \mu\text{m}$ .<sup>12</sup> Therefore, it can be expected that FeSb<sub>2</sub> thin films may have a much lower  $\kappa_L$  than the

bulk material due to surface and grain-boundary scattering of phonons and thus a remarkably enhanced  $ZT$  at low temperature. Here, we report the thermoelectric properties of FeSb<sub>2</sub> films grown by direct-current (dc) magnetron sputtering. Polycrystalline highly  $\langle 101 \rangle$ -textured FeSb<sub>2</sub> films were grown to a thickness of  $\sim 600 \text{ nm}$  on quartz substrates. The transport properties of these FeSb<sub>2</sub> films have been studied together with the properties of FeSb<sub>1.98</sub>Te<sub>0.02</sub> and FeSb<sub>2</sub> single crystals.

## II. EXPERIMENTAL MEASUREMENTS

In this work, FeSb<sub>2</sub> films were grown on quartz (0001) wafers ( $14 \times 14 \text{ mm}^2$ ) by sputtering a specifically prepared compound target. The target (diameter: 25.4 mm; thickness: 3.2 mm) was made by heating 99.99% Fe chips and 99.9999% Sb powder in stoichiometric ratios of 1:2 in a corundum crucible for a reaction and subsequent annealing in an induction furnace with  $\sim 1 \text{ MPa}$  Ar atmosphere for 3 h. X-ray powder diffraction (XRD) analysis showed that the target mainly consisted of FeSb<sub>2</sub> with trace amounts of FeSb, Fe, and Sb. The sputtering system was equipped with a magnetron (power-control mode at a dc power of 10 W, AJA International) that was placed at a distance of 100 mm from the substrate along its normal. The base pressure of the chamber was approximately  $1 \times 10^{-5} \text{ Pa}$ . The sputtering gas was Ar (99.9996%). Optimized growth conditions for nearly phase-pure FeSb<sub>2</sub> films were found to be a substrate temperature of  $\sim 350 \text{ }^\circ\text{C}$ , Ar pressure of  $\sim 0.6 \text{ Pa}$ , and growth time of 3 h. The reproducibility of the deposition process for FeSb<sub>2</sub> films was demonstrated by producing tens of samples using several compound targets. The as-deposited samples were characterized and analyzed by scanning electron microscopy (SEM, Nova600 NanoLab, FEI) with energy dispersive x-ray (EDX) analysis, XRD (D8 Discover, Bruker AXS) in  $\theta$ - $2\theta$  geometry with Cu  $K_\alpha$  radiation, and Ruther-

<sup>a)</sup>Author to whom correspondence should be addressed. Electronic mail: bo@chem.au.dk.

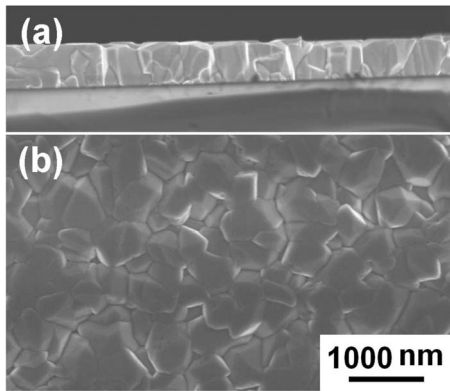


FIG. 1. (a) Cross-section and (b) top view SEM images of an FeSb<sub>2</sub> film produced at 350 °C for 3 h. The scale bar applies to both SEM images.

ford backscattering spectroscopy (RBS, using 2 MeV <sup>4</sup>He<sup>+</sup> and a scattering angle of 161°). The RBS spectra were simulated using the SIMNRA software.<sup>22</sup>

The transport properties of the films were measured using a Quantum Design physical property measurement system (PPMS). Resistivity and Seebeck coefficient were measured simultaneously in the thermal transport option using a standard four-point setup. Wires were mounted on the sample using conducting silver epoxy. Steady state measurements were used at temperatures below 80 K, while the quasi-steady-state approach used in the PPMS was applied above this temperature. The Hall resistivity ( $\rho_H$ ) was measured as function of the magnetic field ( $B$ ) in the ac transport option. Wires were mounted on the film using conducting silver paste. At each magnetic field,  $\rho_H$  was measured in two opposite directions of magnetic field in order to eliminate resistive contribution. Hall coefficient ( $R_H$ ) was determined from  $\rho_H = R_H B$ .

For comparison, thermoelectric properties of FeSb<sub>1.98</sub>Te<sub>0.02</sub> single crystals were also measured on the PPMS. The FeSb<sub>1.98</sub>Te<sub>0.02</sub> single crystals were synthesized by a self-flux method using 99.9999% Sb, 99.999% Te, and 99.98% Fe. The elements were mixed in a 8:92 molar ratio, i.e., Fe<sub>8</sub>(Sb/Te)<sub>92</sub>, and heated to 1000 °C, cooled at 60 °C h<sup>-1</sup> to 750 °C, and subsequently cooled at a rate of 1 °C h<sup>-1</sup> to 550 °C. The remaining flux was removed by centrifuging at 680 °C and subsequent immersion into concentrated hydrochloric acid.

### III. RESULTS

Figure 1 presents representative cross-section and top view SEM images of FeSb<sub>2</sub> films grown at 350 °C for 3 h. The images show that the films are dense, uniform, and continuous. The lateral crystallite sizes of the films are 400–600 nm. The film thickness is ~600 nm. EDX results showed that Fe and Sb were the only two elements present in the film (within the detection limit, shown in the supplemental material<sup>23</sup>). Quantitative EDX analysis revealed that the Fe:Sb atomic ratio in the films is about 1:2 and very close to the reference EDX results from an FeSb<sub>2</sub> single crystal

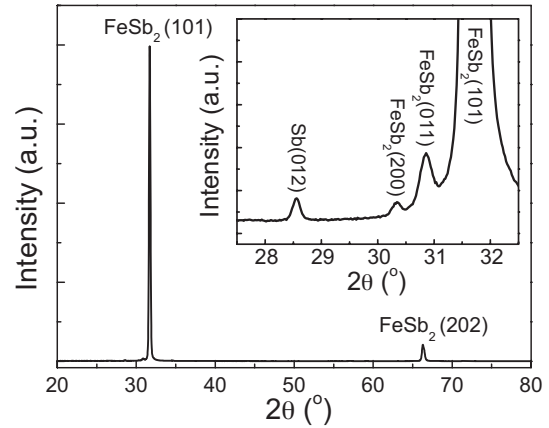


FIG. 2. XRD pattern from the film sample grown at 350 °C for 3 h. The FeSb<sub>2</sub> (101) and (202) peaks dominate the whole XRD pattern. The inset shows the enlarged XRD pattern around  $2\theta=30^\circ$ . A weak peak from elemental Sb located at  $2\theta=28.8^\circ$  is identified.

sample studied in Ref. 12. The film compositions were further verified by RBS, which also gave an Fe:Sb ratio of approximately 1:2.

Figure 2 shows a  $\theta$ - $2\theta$  XRD pattern of an FeSb<sub>2</sub> film. The FeSb<sub>2</sub> (101) and (202) peaks dominate the whole XRD pattern, showing that the FeSb<sub>2</sub> films are highly oriented along the  $\langle 101 \rangle$  direction. A very weak peak located at 28.8° presented in the enlarged XRD pattern (the upper right inset of Fig. 2) comes from elemental Sb, indicating the existence of trace amounts of Sb inside the film. The possible effects of this Sb impurity on the properties of FeSb<sub>2</sub> films will be discussed below.

The XRD, SEM, and EDX results show that the as-deposited films are nearly phase-pure and highly  $\langle 101 \rangle$ -textured. Thermoelectric transport properties of such an FeSb<sub>2</sub> film are presented in Fig. 3. Properties of an FeSb<sub>2</sub> bulk single crystal<sup>12</sup> and an FeSb<sub>1.98</sub>Te<sub>0.02</sub> single crystal along the  $a$ -axis are also presented for comparison. At  $T < 165$  K,  $S$  of the FeSb<sub>2</sub> film presents negative values indicating an  $n$ -type conductivity, and the maximum absolute value of  $S \sim 160 \mu\text{V K}^{-1}$  occurs at  $\sim 50$  K. At  $T > 165$  K,  $S$  changes to positive values and increases with  $T$  to  $\sim 34 \mu\text{V K}^{-1}$  at room temperature (RT). This  $S$  value of the FeSb<sub>2</sub> film at RT is consistent with the results for FeSb<sub>2</sub>

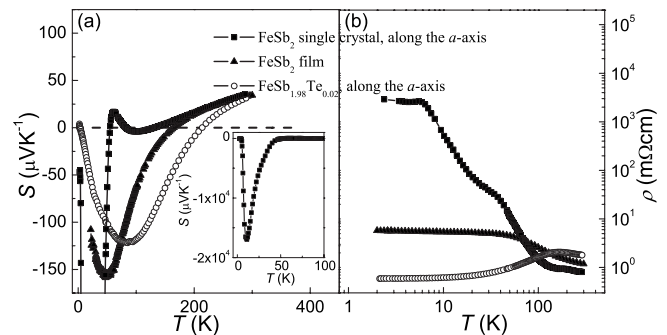


FIG. 3. (a) Seebeck coefficient ( $S$ ) and (b) resistivity ( $\rho$ ) of an FeSb<sub>2</sub> film as function of temperature ( $T$ ). For comparison,  $\rho(T)$  and  $S(T)$  of an FeSb<sub>2</sub> single crystal (Ref. 12) and an FeSb<sub>1.98</sub>Te<sub>0.02</sub> crystal along the  $a$ -axis are also presented. The inset of (a) shows the full range of  $S(T)$  of the FeSb<sub>2</sub> single crystal along the  $a$ -axis.

polycrystalline and single crystals in the literature, where  $S$  was reported to be  $\sim 31\text{--}34 \mu\text{V K}^{-1}$  at 300 K.<sup>9–12</sup> The measured  $S(T)$  of the  $\text{FeSb}_{1.98}\text{Te}_{0.02}$  crystal along the  $a$ -axis is very similar to that of the  $\text{FeSb}_2$  film: the maximum absolute value of  $S \sim 120 \mu\text{V K}^{-1}$  occurs at  $\sim 80$  K;  $S$  changes to positive values at  $T > 210$  K and increases with  $T$  to  $\sim 32 \mu\text{V K}^{-1}$  at RT. Note that although the maximum absolute value of  $S$  of the  $\text{FeSb}_2$  film is much lower than that of the  $\text{FeSb}_2$  single crystals [the inset of Fig. 3(a)], their temperature dependence is quite similar. The similar behaviors of  $S(T)$  of the  $\text{FeSb}_2$  film, the  $\text{FeSb}_2$  single crystal, and the  $\text{FeSb}_{1.98}\text{Te}_{0.02}$  single crystal imply that the thermoelectric properties of the film are dominated by the intrinsic properties of  $\text{FeSb}_2$  rather than some impurity phase such as elemental Sb.

$\rho(T)$  of the  $\text{FeSb}_2$  film measured simultaneously with the Seebeck coefficient is shown in Fig. 3(b). At RT, the measured resistivity of the  $\text{FeSb}_2$  film is about  $1.2 \text{ m}\Omega \text{ cm}$ , similar to the values obtained from the  $\text{FeSb}_2$  single crystal ( $\sim 0.85 \text{ m}\Omega \text{ cm}$ ) and the  $\text{FeSb}_{1.98}\text{Te}_{0.02}$  crystal ( $\sim 1.8 \text{ m}\Omega \text{ cm}$ ). It is notable that the temperature dependence of the resistivity of these three samples presents much difference.  $\rho(T)$  of both the film and the  $\text{FeSb}_2$  single crystal decreases with increasing  $T$ . However, the ratio of  $\rho(2 \text{ K})$  to  $\rho(300 \text{ K})$  for the film is  $\sim 5$ , which is much smaller than that of the  $\text{FeSb}_2$  single crystal ( $\sim 10\,000$ ). In contrast,  $\rho(T)$  of the  $\text{FeSb}_{1.98}\text{Te}_{0.02}$  single crystal increases with temperature of up to  $\sim 160$  K after which it decreases. Based on the Arrhenius plot, i.e.,  $\ln \rho$  as a function of reciprocal temperature (shown in the supplemental material<sup>23</sup>), the activation energy of the  $\text{FeSb}_2$  film below 3 K is calculated as  $\sim 0.01 \text{ meV}$ , which is probably due to extrinsic impurity states. At  $T > 100$  K, the Arrhenius plot leads to an activation energy of  $\sim 9.65 \text{ meV}$ , which is lower than previously published values on polycrystalline and single crystals of  $\text{FeSb}_2$ .<sup>9,12</sup>

In order to further explore the thermoelectric transport properties of the  $\text{FeSb}_2$  films, Hall measurements were performed on the  $\text{FeSb}_2$  film and the  $\text{FeSb}_{1.98}\text{Te}_{0.02}$  single crystal. Figure 4(a) shows the calculated charged carrier concentrations ( $n$ ) of the  $\text{FeSb}_2$  film and the  $\text{FeSb}_{1.98}\text{Te}_{0.02}$  single crystal by applying a single parabolic band model. The obtained  $n$  of the  $\text{FeSb}_2$  film ( $4\text{--}10 \times 10^{20} \text{ cm}^{-3}$  at 10–50 K) and the  $\text{FeSb}_{1.98}\text{Te}_{0.02}$  single crystal ( $\sim 2 \times 10^{21} \text{ cm}^{-3}$  at 10–50 K) is much higher than that of the  $\text{FeSb}_2$  single crystal ( $\sim 10^{15} \text{ cm}^{-3}$  at 10 K).<sup>24</sup> These results are consistent with the resistivity measurements of these three samples at low temperature shown in Fig. 3(b). The much reduced maximum absolute value of  $S$  of the  $\text{FeSb}_2$  film is most likely due to its very high carrier concentration.

The Hall carrier mobilities of the  $\text{FeSb}_2$  film and the  $\text{FeSb}_{1.98}\text{Te}_{0.02}$  single crystal are presented in Fig. 4(b).  $\text{FeSb}_2$  single crystals have been reported to have carrier mobilities of up to  $\sim 10^5 \text{ cm}^2 \text{ V}^{-1} \text{ s}^{-1}$ , suggesting application of  $\text{FeSb}_2$  in high-speed electronic devices.<sup>25</sup> However, the Hall carrier mobility of the  $\text{FeSb}_2$  films in this work never exceeds  $10 \text{ cm}^2 \text{ V}^{-1} \text{ s}^{-1}$ . This difference can mainly be attributed to the increase in  $n$  since the mobility is of comparable magnitude to the value observed at similar  $n$  in the  $\text{FeSb}_{1.98}\text{Te}_{0.02}$

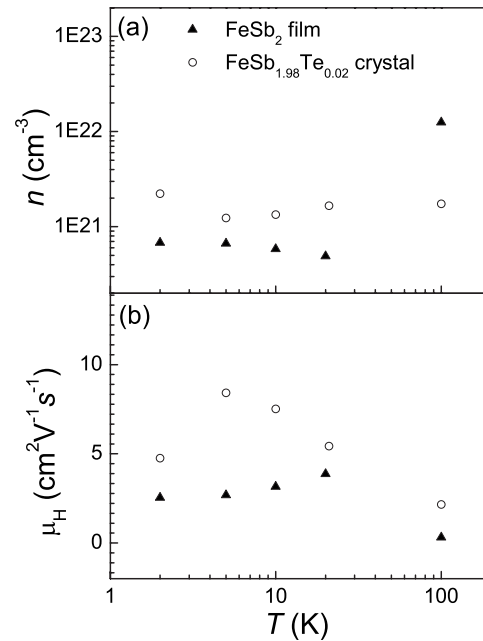


FIG. 4. (a) The calculated carrier concentrations and (b) Hall carrier mobilities of the  $\text{FeSb}_2$  film and the  $\text{FeSb}_{1.98}\text{Te}_{0.02}$  crystal by applying a single parabolic band model.

single crystal. In addition, charge carrier scattering due to grain boundaries, structural defects, and impurities in the  $\text{FeSb}_2$  film could also play an important role.

The XRD results reveal trace amount of elemental Sb in the  $\text{FeSb}_2$  films (the inset of Fig. 2). As a metal, Sb could stay in the crystal boundaries and together with other defects and impurities lead to a very high carrier concentration of the  $\text{FeSb}_2$  films. The resistivity of Sb films was reported to increase with increasing temperature between 10 and 250 K,<sup>26</sup> whereas the resistivity of the  $\text{FeSb}_2$  film in this work decreases with increasing temperature [Fig. 3(b)]. This implies that although the Sb impurity could be an important reason for the reduced resistivity and thermopower in the films at low temperature, the thermoelectric transport properties of the  $\text{FeSb}_2$  films are still dominated by the intrinsic properties of  $\text{FeSb}_2$ .

Experiments to reduce the carrier concentration and increase the crystallite sizes of  $\text{FeSb}_2$  films and to ultimately grow single crystalline films clearly merit further study. Such single crystalline  $\text{FeSb}_2$  films are expected to have a colossal Seebeck coefficient and a giant carrier mobility as observed in  $\text{FeSb}_2$  single crystals but a much reduced thermal conductivity, thus providing a promising TM for solid state cooling devices as well as an excellent material for high-speed electronics.

#### IV. CONCLUSION

In summary, highly  $\langle 101 \rangle$ -textured  $\text{FeSb}_2$  films were produced by magnetron sputtering. Their thermoelectric transport properties were studied by comparing the properties of  $\text{FeSb}_{1.98}\text{Te}_{0.02}$  and  $\text{FeSb}_2$  single crystals. It is revealed that the intrinsic properties of  $\text{FeSb}_2$  dominate the thermoelectric properties of the  $\text{FeSb}_2$  films. However, the large carrier concentration of the  $\text{FeSb}_2$  films leads to a maximum absolute

value of  $S \sim 160 \mu\text{V}/\text{K}$  at 50 K. These results improve the understanding of the extraordinary thermoelectric properties of  $\text{FeSb}_2$ , and they suggest that it may indeed be possible to exploit  $\text{FeSb}_2$  in thin film devices.

## ACKNOWLEDGMENTS

We thank Dr. Anders Bienten for fruitful discussions. Financial support from the Danish Strategic Research Council and the Lundbeck Foundation is gratefully acknowledged. P.E. acknowledges support from the Carlsberg Foundation, the Swedish Research Council (VR), and the Swedish Agency for Innovation Systems (VINNOVA).

- <sup>1</sup>F. J. DiSalvo, *Science* **285**, 703 (1999).
- <sup>2</sup>G. J. Snyder and E. S. Toberer, *Nature Mater.* **7**, 105 (2008).
- <sup>3</sup>S. B. Riffat and X. L. Ma, *Appl. Therm. Eng.* **23**, 913 (2003).
- <sup>4</sup>W. M. Yim and A. Amith, *Solid-State Electron.* **15**, 1141 (1972).
- <sup>5</sup>D. Y. Chung, T. Hogan, P. Brazis, M. Rocci-Lane, C. Kannewurf, M. Bastea, C. Uher, and M. G. Kanatzidis, *Science* **287**, 1024 (2000).
- <sup>6</sup>B. Poudel, Q. Hao, Y. Ma, Y. C. Lan, A. Minnich, B. Yu, X. Yan, D. Z. Wang, A. Muto, D. Vashaee, X. Y. Chen, J. M. Liu, M. S. Dresselhaus, G. Chen, and Z. Ren, *Science* **320**, 634 (2008).
- <sup>7</sup>C. Petrovic, Y. Lee, T. Vogt, N. D. Lazarov, S. L. Bud'ko, and P. C. Canfield, *Phys. Rev. B* **72**, 045103 (2005).
- <sup>8</sup>A. Perucchi, L. Degiorgi, R. W. Hu, C. Petrovic, and V. F. Mitrovic, *Eur. Phys. J. B* **54**, 175 (2006).
- <sup>9</sup>A. Bienten, K. H. Madsen, S. Johnsen, and B. B. Iversen, *Phys. Rev. B* **74**, 205105 (2006).
- <sup>10</sup>N. K. Abrikosov and L. I. Petrova, *Inorg. Mater.* **25**, 1087 (1989).
- <sup>11</sup>L. I. Petrova, N. K. Abrikosov, L. D. Dudkin, V. M. Sokolova, and V. V. Musaelyan, *Inorg. Mater.* **26**, 1023 (1990).
- <sup>12</sup>A. Bienten, S. Johnsen, G. K. H. Madsen, B. B. Iversen, and F. Steglich, *Europhys. Lett.* **80**, 17008 (2007).
- <sup>13</sup>G. D. Mahan, *Solid State Phys.* **51**, 81 (1998).
- <sup>14</sup>K. F. Hsu, S. Loo, F. Guo, W. Chen, J. S. Dyck, C. Uher, T. Hogan, E. K. Polychroniadis, and M. G. Kanatzidis, *Science* **303**, 818 (2004).
- <sup>15</sup>M. Christensen, A. B. Abrahamsen, N. B. Christensen, F. Juranyi, N. H. Andersen, K. Lefmann, J. Andreasson, C. R. H. Bahl, and B. B. Iversen, *Nature Mater.* **7**, 811 (2008).
- <sup>16</sup>B. C. Sales, D. Mandrus, and R. K. Williams, *Science* **272**, 1325 (1996).
- <sup>17</sup>A. I. Hochbaum, R. K. Chen, R. D. Delgado, W. J. Liang, E. C. Garnett, M. Najarian, A. Majumdar, and P. D. Yang, *Nature (London)* **451**, 163 (2008).
- <sup>18</sup>X. F. Qiu, L. N. Austin, P. A. Muscarella, J. S. Dyck, and C. Burda, *Angew. Chem., Int. Ed.* **45**, 5656 (2006).
- <sup>19</sup>T. Ikeda, L. A. Collins, V. A. Ravi, F. S. Gascoin, S. M. Haile, and G. J. Snyder, *Chem. Mater.* **19**, 763 (2007).
- <sup>20</sup>R. Venkatasubramanian, E. Siilvola, T. Colpitts, and B. O'Quinn, *Nature (London)* **413**, 597 (2001).
- <sup>21</sup>M. S. Dresselhaus, G. Chen, M. Y. Tang, R. G. Yang, H. Lee, D. Z. Wang, Z. F. Ren, J.-P. Fleurial, and P. Gogna, *Adv. Mater. (Weinheim, Ger.)* **19**, 1043 (2007).
- <sup>22</sup>M. Mayer, *Nucl. Instrum. Methods Phys. Res. B* **194**, 177 (2002).
- <sup>23</sup>See EPAPS supplementary material at <http://dx.doi.org/10.1063/1.3155800> for supplemental material for thermoelectric transport properties of highly oriented  $\text{FeSb}_2$  thin films.
- <sup>24</sup>P. Sun, N. Oeschler, S. Johnsen, B. B. Iversen, and F. Steglich, *J. Phys.: Conf. Ser.* **150**, 012049 (2009).
- <sup>25</sup>R. Hu, V. F. Mitrovic, and C. Petrovic, *Appl. Phys. Lett.* **92**, 182108 (2008).
- <sup>26</sup>B. A. Hermann, I. Didschuns, P. Haier, M. Kopp, N. Esser, U. Resch-Esser, W. Richter, and K. Luders, *Thin Solid Films* **275**, 125 (1996).